Supporting Information for

Multilevel Ultra-Fast Flexible Nanoscale Non-Volatile Hybrid Graphene Oxide - Titanium Oxide Memories

*V. Karthik Nagareddy,[†] Matthew D. Barnes,[†] Federico Zipoli,[§] Khue T. Lai,[†] Arseny M. Alexeev,[†] Monica Felicia Craciun,[†] and C. David Wright[†]**

[†]Centre for Graphene Science, College of Engineering, Mathematics and Physical Sciences, Harrison Building, North Park Road, University of Exeter, Exeter EX4 4QF, UK.
[§]IBM Research–Zurich, Säumerstrasse 4, 8803 Rüuschlikon, Switzerland.

*Address correspondence to C.D.W (email: david.wright@exeter.ac.uk)

Supporting Information - Methods and Results

C-AFM electrical switching measurements

The electrical switching measurements were performed using a Bruker Innova SPM system with two complementary modes of operation: a low frequency mode equipped with a variable gain current amplifier and a high frequency mode with no amplifying device. The low frequency mode is used for C-AFM imaging and for I-V characterization of the sample. The high frequency mode uses a programmable function generator for fine control of the electrical excitation. This arrangement allows relatively fast pulses of variable and controlled amplitude to be applied to the cells, while also allowing for the cell resistance to be measured at DC after the application of each pulse. A 50 Ω surface mount resistor was positioned right next to the C-AFM tip module to provide a proper impedance matching between the pulse generator and the tip. A 4.7 kΩ resistor was placed in series with the sample/device and acted as current limiter, protecting the tip and the sample from any sudden increase in current during the application of a pulse or during an I-V scan. In Figure S1 below we show the results of repeated I-V scans of a single cell, while in Figure S2 we show the form of the voltage pulses typically used for pulsed switching experiments. For more information on the experimental set-up see Ref.[1]

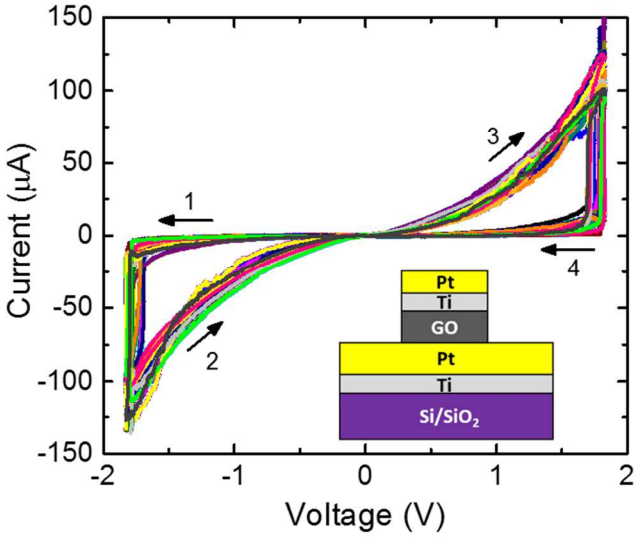

Supporting Figure S1. The I-V characteristics of a 75 nm diameter memory cell with 100 switching cycles superimposed on top of each other. It can be seen that the repeatability is good, as corroborated by pulsed switching endurance measurements shown in Figure 2 of the main manuscript.

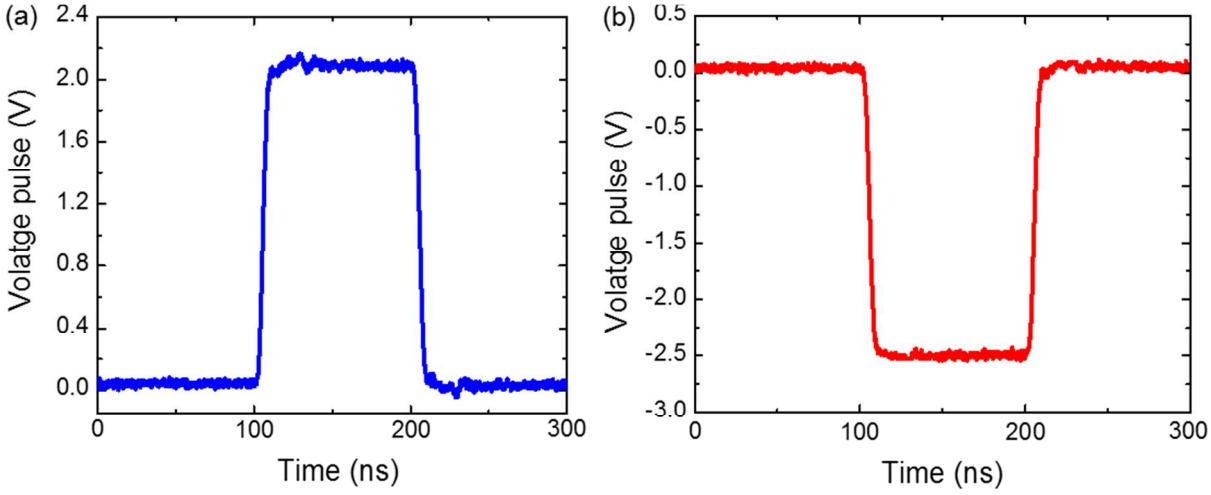

Supporting Figure S2. Typical (a) SET and (b) RESET pulses, here of 100 ns duration, used for reversible pulsed-switching of memory cells.

The bi-polar I-V sweeps such as those in Figure S1 above were initially performed to verify the switching capability of the fabricated GO/TiO_x memory cells. After this initial characterization, the performance (i.e. endurance, retention times and switching speeds) of these fabricated cells were tested by using pulsed excitations, which is common practice when assessing the device performance for practical memory applications. A Tektronix AFG3101 and Avtech AVMR-2D-B arbitrary pulse function generators were used to switch the device between LRS (SET) and HRS (RESET) states by applying suitable voltage pulses of different widths and amplitudes. Typical SET and RESET pulses of 100 ns full-width-at-half-maximum as captured from the oscilloscope (Lecroy wavefront 640Z) are shown in Figure S2. By careful control of the pulse amplitudes we could realise multi-bit memory states as discussed below. After the application of pulse (SET or RESET), the resistance of the memory cell was extracted using the C-AFM in DC mode by performing I-V sweeps at very low biases (-0.6 to +0.6 V) and collecting the current via the current amplifier (DLPCA-200, Femto) that is integral to the C-AFM equipment.

Memory cell characterization results

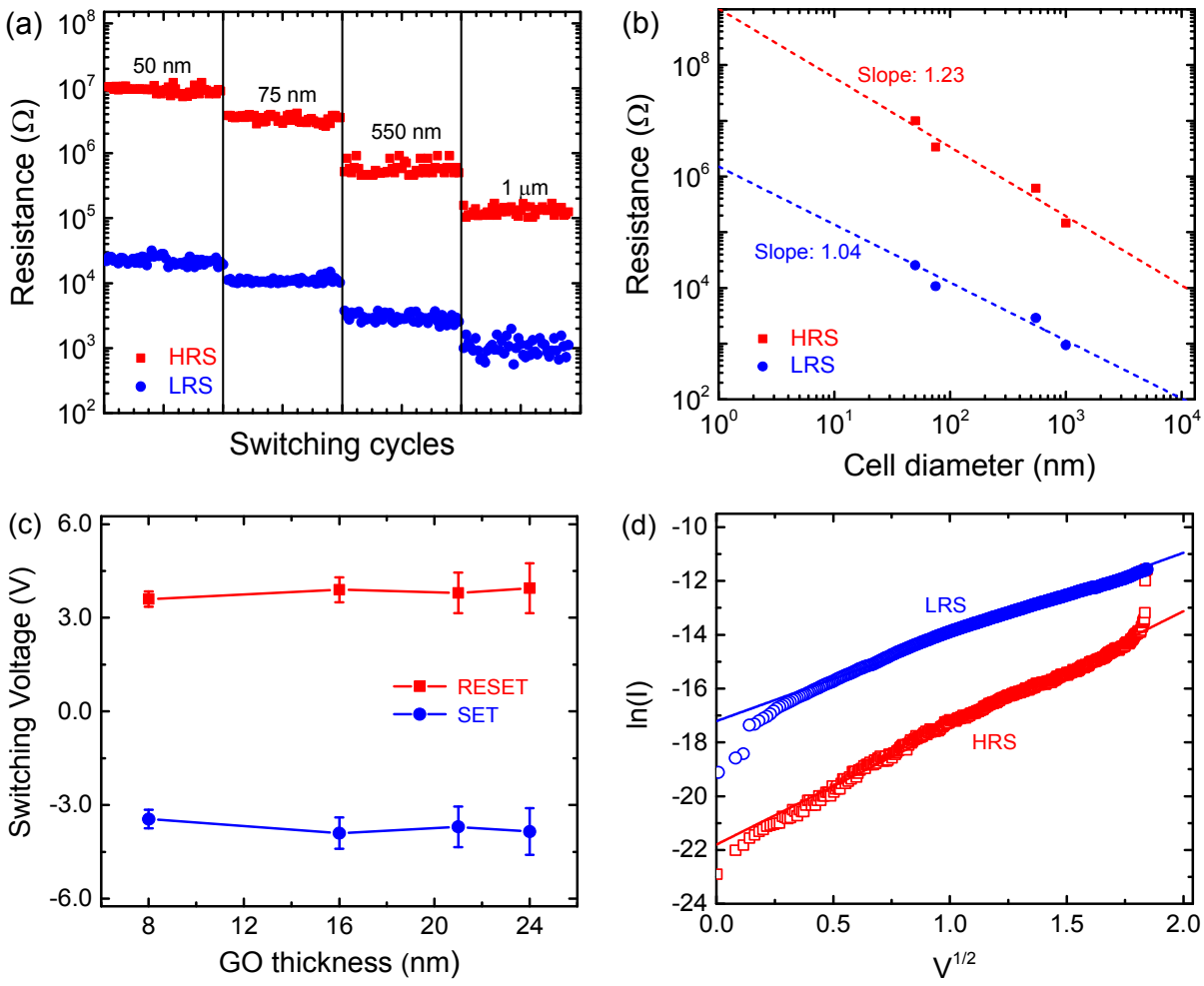

Supporting Figure S3. (a) and (b) show that the cell resistance scales with cell area in both the HRS and LRS states, pointing to an interfacial dominated switching mechanism rather than a filamentary process. (c) shows the device switching voltages as function of GO thickness (~ 8 nm to ~ 24 nm). As can be seen, negligible change in switching voltages was observed with increasing GO layer thickness, demonstrating the interfacial nature of the switching mechanism in our hybrid Ti/GO memories. (d) Shows that cells in both the HRS and LRS states display a good linear fit between the logarithm of the current and the square root of the applied voltage, indicating that a Schottky emission process dominates the carrier transport for the device in the low voltage (pre-switching) region.

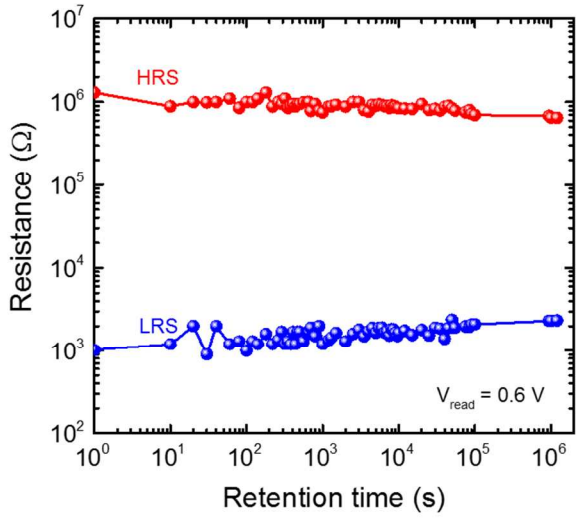

Supporting Figure S4. Extended retention time performance of our GO memories showing a resistance window of nearly 3 orders of magnitude still exists even after 6 months stored at room temperature (note that up to 10^5 seconds the devices were stored in an open lab environment; from 10^5 seconds onwards they were still stored in the lab but in a desiccator).

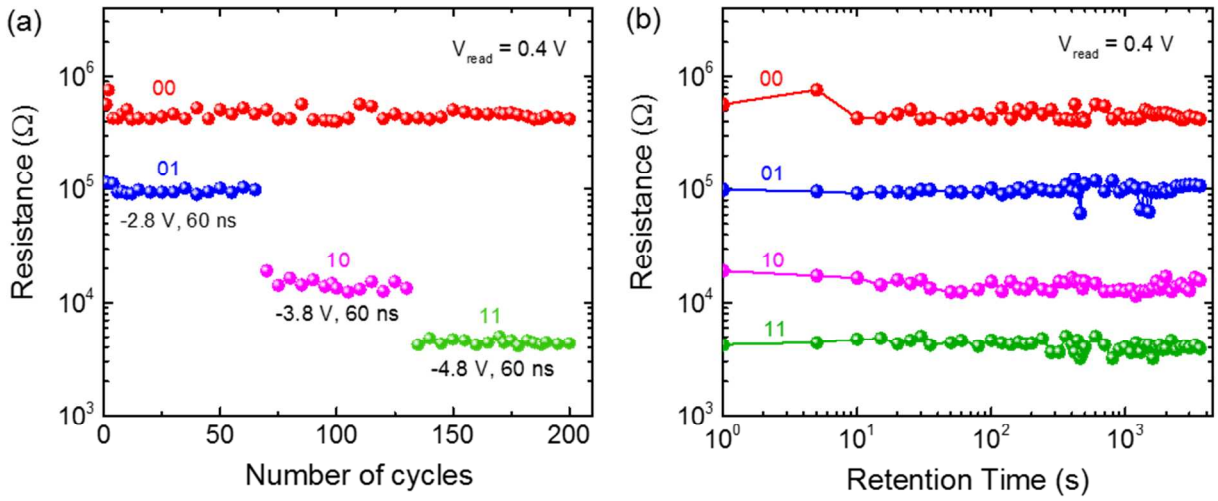

Supporting Figure S5. (a) The writing and (b) the retention behaviour of 8 nm thick multilevel GO memory cells fabricated on a flexible PEN (polyethylene naphthalate) substrate.

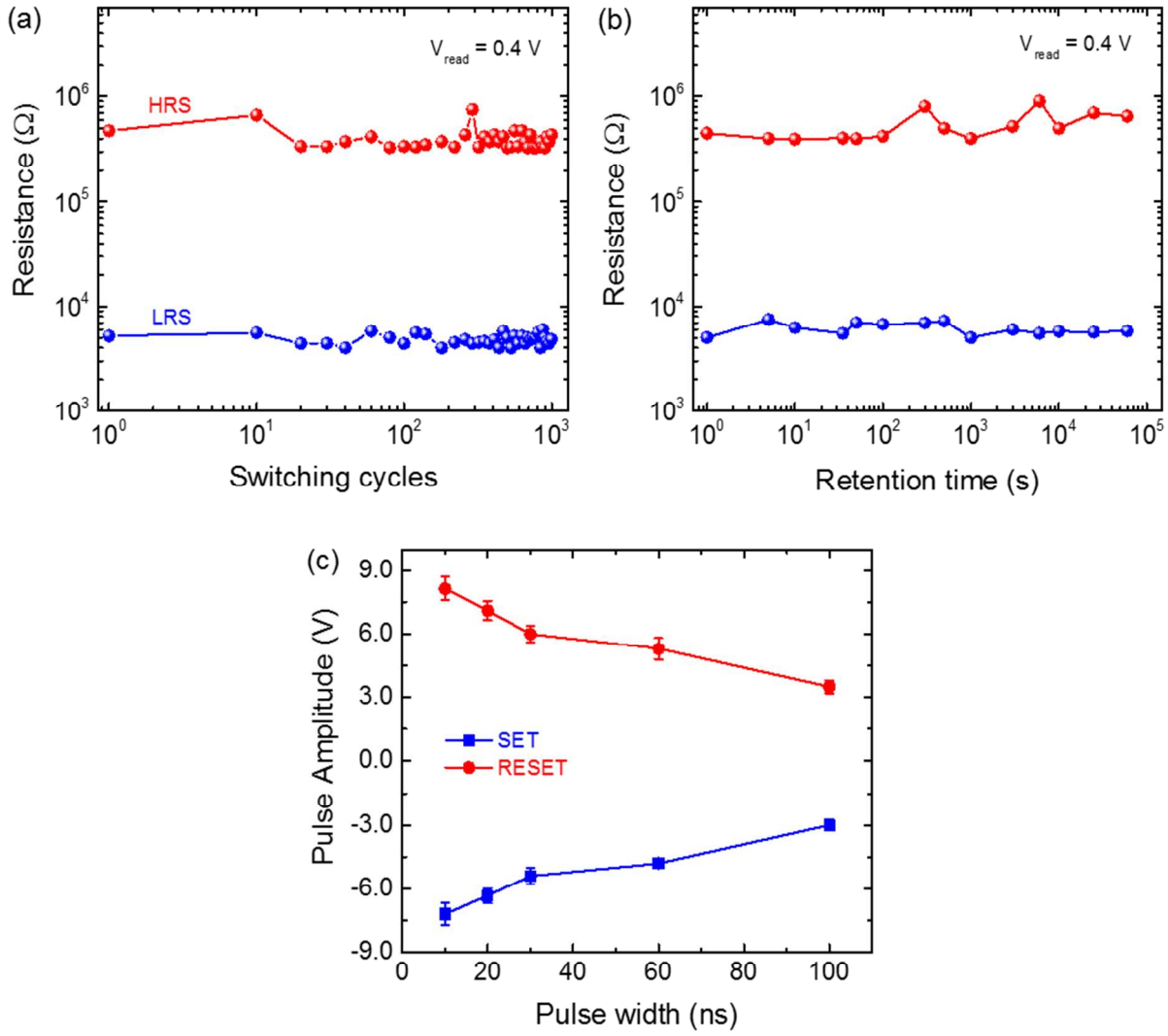

Supporting Figure S6. (a) The endurance, (b) retention and (c) switching speed characteristics for 8 nm thick GO memory cells fabricated on a flexible PEN (polyethylene naphthalate) substrate.

Switching mechanism and the role of the GO and TiO_x

Both GO and TiO_x play an active role in the switching process in our memory devices. Indeed, cells fabricated using a Pt/GO/Pt structure alone did not show any reversible switching (see Figure S7). We also carried out additional Raman spectral analysis to clearly identify the change in chemical and structural state of our GO/TiO_x memory structures under upon switching.

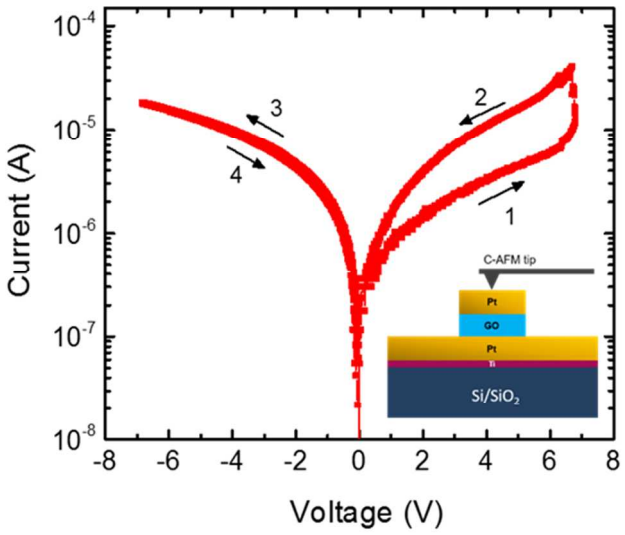

Supporting Figure S7. I-V characteristics of a Pt/GO/Pt cell; no reversible switching was observed.

Supporting Figure S8a shows the schematic illustration for measuring the Raman spectra of a selected GO/TiO_x memory cell. For the purpose of Raman characterisation, memory cells (5 µm diameter) consisting of ultra-thin top electrodes with ~ 1.5 nm Pt capping layer and ~ 4.5 nm Ti layer were deposited on GO, which allows direct and non-destructive access to the Ti/GO interfacial region to acquire the Raman spectra in both HRS and LRS states without the need for removing the top electrode (note, to improve the signal-to-noise ratio, long acquisition times (300 s) as well as Savitzky-Golay smoothing was performed on all the acquired spectra). Any change in chemical and structural composition of the GO film (i.e. reduction and oxidation) before and after switching can be clearly seen in the Raman spectrum by monitoring the relative intensity of D and G peaks.[2] The D peak originates due to structural imperfections to the graphene lattice created by the attachment of hydroxyl and epoxy functional groups on the graphene basal plane, whilst the G peak is due to the first-order scattering of the E_{2g} phonon mode at the Brillouin Zone centre.[3] The intensity of the D peak is related to the size of the in-

plane sp^2 domains and its increase is a general indicator of formation of more sp^2 domains due to the removal of attached O-groups from the GO, leading to reduced GO (rGO) state. The relative intensity ratio of both D and G peaks (I_D/I_G) is a measure of degree of disorder in GO and is inversely proportional to the average size of the sp^2 domains. The increase in this intensity ratio is a general indicator of formation of more sp^2 domains due to the removal of attached O-groups from the GO, leading to reduced GO (rGO) state.

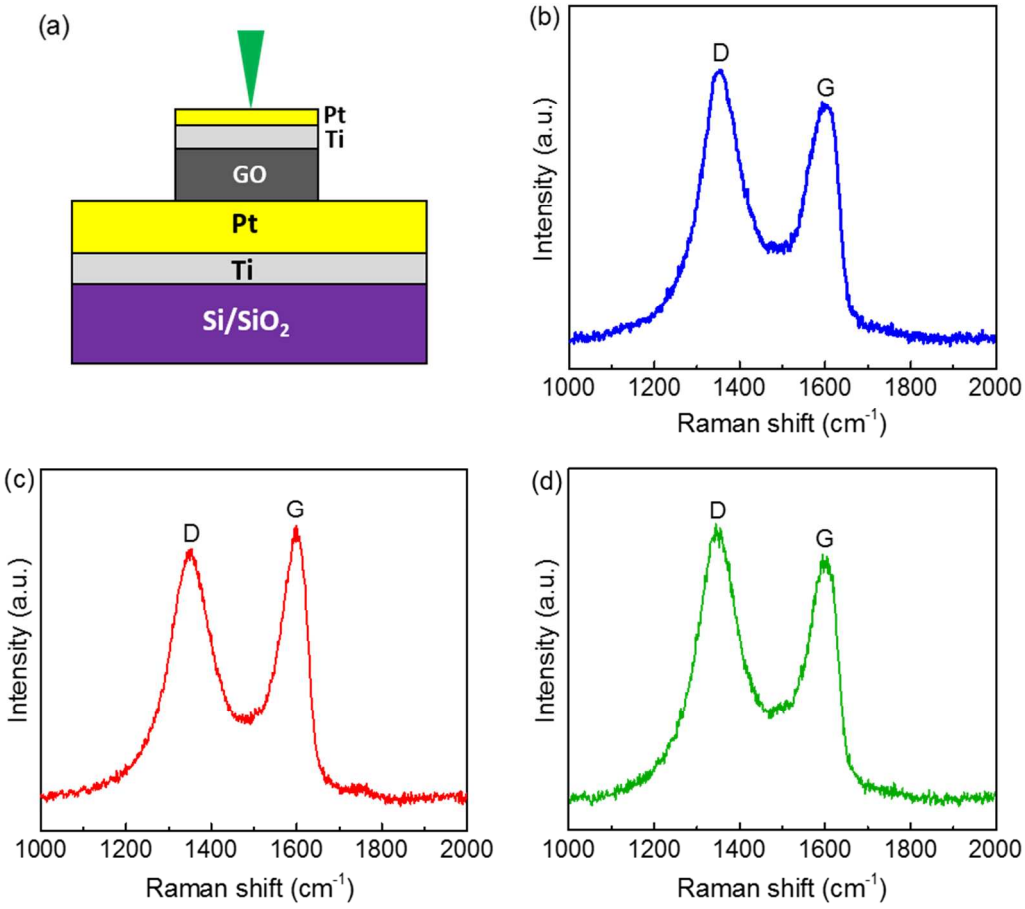

Supporting Figure S8. (a) Schematic illustration of Pt/Ti/GO/Pt memory structure used for non-destructive measurement of Raman spectra of a cell, Acquired Raman spectra of the D and G bands when the cell is in (a) the pristine, (c) the LRS and (d) the HRS state.

The results of Supporting Figure S8 corroborate the view that when the Ti metal film is deposited on top of the oxygen-rich GO film, the Ti atoms take O-groups from the first few nanometres of the GO, leading to the formation of an TiO_x amorphous interface layer (see also Figure S9), such that the pristine state of the cell is high-resistance. As the GO loses O-groups to

Ti, the first few nanometres of GO will now be in a reduced GO (rGO) state. The Rama spectra of this pristine memory state (with no switching performed) is shown in Fig. S8b and displays characteristic D and G peaks at around 1352 cm^{-1} and 1600 cm^{-1} with an I_D/I_G ratio of 1.15. By applying a negative bias to the top electrode the device switches to the low resistance state (LRS or SET) state and the D/G intensity ratio decreases to 0.89 (see Fig. S8c), implying the local re-oxidation of GO by out-diffusion of oxygen ions from the TiO_x layer. However, when a reverse (positive) bias was applied to the top electrode, the I_D/I_G ratio again increases to ~ 1.11 (see Fig. S8d) and the cell was reset to the HRS state due to the reduction of GO and subsequent re-oxidation of Ti/TiO_x layer. Such redox reactions between Ti and GO were also confirmed by XPS measurements shown in the main text, where the TiO_x peaks were reduced in amplitude (see main text Fig. 5c Ti2p spectra) after switching the device to the low-resistance state, while a simultaneous increase in the C-O/C=O peak (see main text Figure 5a C1s spectra) was observed, demonstrating the recovery of GO from its previous rGO state.

Note, this reduction and oxidation of GO was only observed when the Ti (chemically active) layer was in contact with the GO layer, whilst no change in GO structural or chemical state was seen when only a Pt (chemically inactive) layer was deposited. Thus the switching mechanism in these GO/TiO_x hybrid cells involve active participation of both GO and TiO_x layers, where the transfer of oxygen atoms takes place under an external electric field.

The origin of multi-bit resistance states observed in our memory devices is attributed to the extent of oxygen atoms transfer from the Ti/TiO_x interface layer to the GO film. For example, in line with the discussion above, when the memory cell is in HRS state (00 state), the first few nanometres of GO will be in a rGO state due to the loss of O-groups to Ti. By, applying a negative voltage pulse to the top electrode with an appropriate amplitude, the back-transfer of oxygen atoms from the Ti/TiO_x interfacial layer to the GO film takes place, effectively setting the cell to LRS state (11 state). However, by controlling the pulse amplitudes, the amount of oxygen transfer from Ti/TiO_x to GO can be controlled in such a way that the rGO at the interface gradually transforms to oxygen-rich GO, lowering the interfacial energy barrier between Ti and GO, leading to distinct and well resolved multiple resistance states. This multi-bit switching mechanism is also explained via the atomistic simulation results of Supporting Figure S15, where we show optical conductivity (as a proxy for electrical conductivity) versus the degree of oxygen transfer. As can be seen in Figure S15, the optical conductivity (resistivity) decreases

(increases) as the oxygen atoms are transferred from the GO to the titanium and vice versa, see inset of Figure S15c, which is a plot of values of (optical) conductivity at E=0.15 and 0.2 eV versus the oxygen content in GO for structures S1, S2, S3, S4, and S5. Thus, controlled and reversible interfacial oxidation/reduction of the active GO/TiO_x layer with multi-bit states can be achieved by applying appropriate pulse amplitudes to the memory cell

We also note that the switching mechanism in our GO/TiO_x devices is fundamentally different to that of 'conventional' TiO_x-based resistive memories. The current understanding of the switching mechanism in TiO_x-type RRAM devices is that it is a filamentary process that involves the formation of several titanium oxide crystal phases, in particular the rutile and anatase phases, due to localized Joule heating produced during the switching process.[6] Similarly, the formation of magnéli crystal phase has also been linked to the switching mechanism[7]. The formation of such phases requires relatively high temperatures of ~ 600 K for anatase and ~1000 K for rutile, whilst the magnéli phase is formed from the rutile crystal phase. Such high temperatures are certainly not reached in our devices, because if it were then we would permanently reduce our GO film to graphene like material, (as 600 K is high enough to remove majority of the O-groups attached to the graphene sheet) leading undoubtedly to a permanently-switched low-resistance state. Furthermore, the dependence of resistance on device area, that we showed in Figure S3 of this Supporting Information, is a characteristic of a non-filamentary, interface-dependent switching mechanism, again supporting the view that the switching process in our case is not that of 'conventional' TiO_x-type RRAM devices.

More definitively, using Raman spectroscopy we can categorically show that the above Ti-oxide crystal phases associated with conventional TiO_x RRAM switching are not formed in our devices. For example, Figure S9 below shows typical Raman spectra (taken from the literature) of the rutile and anatase crystal phases of TiO_2, where strong peaks are evident at ~ 125 cm^{-1}, ~ 450 cm^{-1} and ~ 600 cm^{-1}. The amorphous TiO_2 phase, however, shows no such distinctive peaks. Raman measurements of our GO/TiO_x memory cells, taken in both the high and low resistance states (and also given in Figure S9), exhibit no evidence of peaks due to any TiO_2 crystal phases, showing only the characteristic response of amorphous TiO_2. Thus, we are confident that the switching mechanism in our devices is based on the reduction and oxidation of GO/TiO_x hybrid structure as described above, and not due to a switching mechanism akin to that of TiO_x-type RRAM devices.

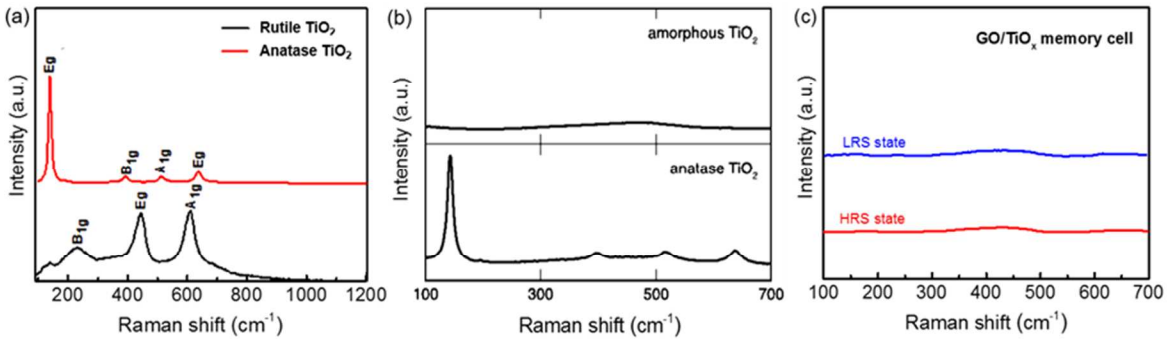

Supporting Figure S9. Raman spectra of (a) rutile and anatase TiO_2 crystal phases taken from Ref.[4] (b) Amorphous and anatase TiO_2 phases taken from Ref.[5] (c) Raman spectra from this work acquired before and after switching the memory cell, revealing only the amorphous like structure.

Supporting Information – Atomistic Simulations

We modeled GO and the Ti/GO interface at the DFT level with two types of systems: large structures using simulation box containing at most 621 atoms. Smaller systems consisting of about one hundred atoms were used for more accurate total energy calculations using a 4x2x1 mesh k-points to accurately sample the Brillouin zone (BZ). Two prototypical systems are illustrated in Supporting Figure S10. The simulation box in Supporting Figure S10a is commensurate with the graphene and titanium lattice parameters with a small mismatch (less than 3%) [[6]]. The BZ integration was performed over a 4×2×1 shifted Monkhorst-Pack mesh a good compromise between computational cost and accuracy. For the large systems, see for example Supporting Fig. S10c, we used only Gamma point of the BZ for energy calculations. Supporting Figs. S11a, S12a, and S13a illustrates three structures used to study the redox reactions at the Ti/GO interface. The GO configuration in Supporting Figure S11a contains epoxy groups obtained after adsorption of oxygen atoms on a clean graphene. The structure in Supporting Figure S12a contains an oxidized graphene layer with a void, produced by removal of carbon atoms. The structure in Supporting Figure S13 contains epoxy and hydroxyl groups. The GO layers have been relaxed in a simulation cell without titanium before being put close to titanium. Upon relaxation most of the epoxy and hydroxyl groups bonded on the side of the graphene exposed to the titanium surface migrated from GO towards titanium. Most of the oxygen atoms were adsorbed at the titanium surface, a few oxygen diffused between the first and the second layers of titanium. The relaxed configurations are illustrated in Supporting Figs. S11c,

S12b, and S13b. We found that the structures of Supporting Figs. S11a, S12a, and S13a with GO layers close to titanium are not even metastable. Migration of the oxygen atoms of GO exposed to the titanium surface is a barrierless process. Supporting Figure S14 compares the binding energy of oxygen atoms at titanium surface and on graphene: oxidation of titanium via oxygen transfer from epoxy groups of GO to titanium in an exothermic process with an energy stabilization of about 5 eV/O-atom.

Supporting Figure S15 presents a comparison of the electronic properties of different Ti/GO interfaces we used to elucidate the link between degree of oxidation of titanium and the resistance of the system. We computed the electron density of state and the optical conductivity to link the structural changes, produced by migration of oxygen between GO and titanium, to the experimentally observed change in resistance in the material. In particular, we used the hybrid functional PBE0, which allows to improve the description of band gap, which is usually underestimated in standard DFT. The optical conductivity σ(E) was computed according to the Kubo-Greenwood formula

$$\sigma(E) = \frac{2\pi\hbar e^2}{3m_e^2 V_{\text{cell}}} \frac{1}{E} \sum_{i,j} (f_i - f_j) |\langle \psi_j | \hat{\boldsymbol{p}} | \psi_i \rangle|^2 \delta(\varepsilon_j - \varepsilon_i - E)$$

where e is the elementary charge, m_e is the electron mass, $\boldsymbol{p}$ is the momentum operator, V_{cell} is the volume of the box, ψ_i are the KS orbitals at the PBE0 level, εi are their corresponding eigenvalues, and f_i and f_j are their occupation numbers of the occupied and empty states, respectively. In this work we use the optical conductivity σ(E) as function of energy E projected along the normal to the Ti/GO interface, $\sigma_z(E)$, in order to decouple the parallel and perpendicular contributions of σ(E) to the interface. Supporting Fig. S11c shows a correlation between $\sigma_z(E)$ and the amount of oxygen in the titanium and GO. More specifically, the conductivity decreases as O atoms move from GO to titanium, see inset of Fig. S15c.

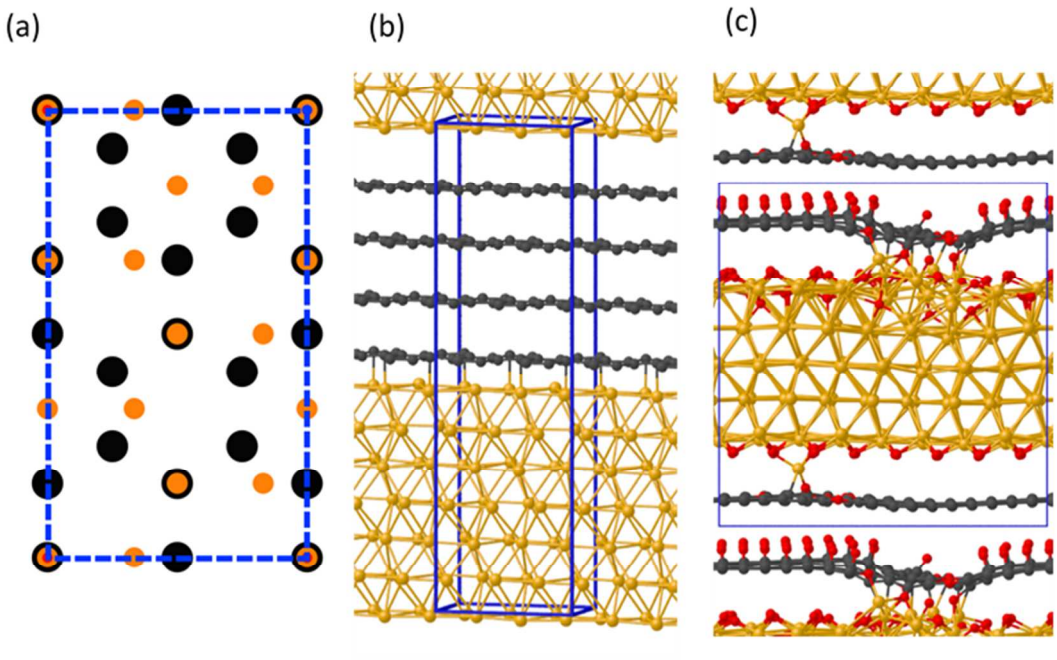

Supporting Figure S10. (a) Top view of the smallest system used to model the titanium / (clean) graphene interface. Only the closest layers of Ti and C atoms are illustrated. The box contains 7 titanium layers and four layers of graphene. The box size is a, b, and c equal to 5.08, 8.80, and 29.98 Å. (b) Lateral view of (a). Each titanium (carbon) layer consists of 6 (8) atoms. (c) Lateral view of one of the largest structures used to model the Ti/GO interface consisting of 621 atoms. Titanium, carbon, and oxygen atoms are indicated in orange, dark grey, and red, respectively. We used 3-dimensional periodic boundary conditions. The simulation box is indicated via blue lines.

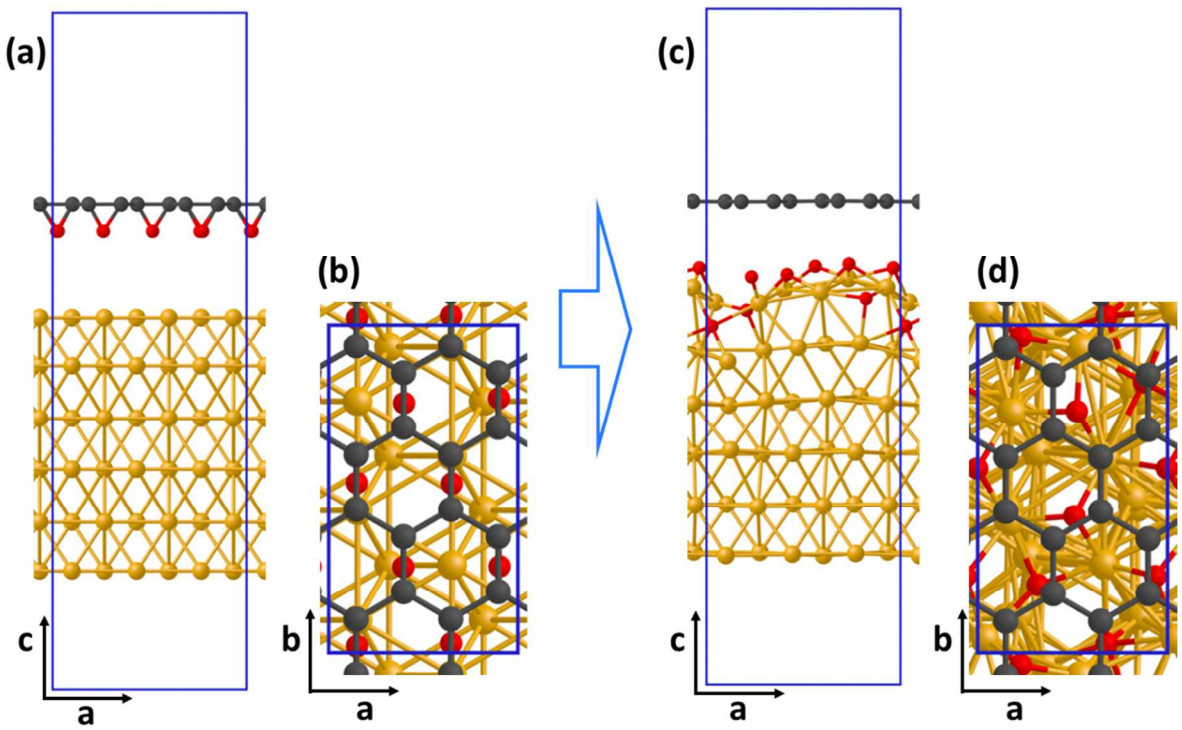

Supporting Figure S11. (a) Side and (b) top view of the initial configuration with a GO layer made of 16 C-atoms with 8 C-O-C epoxy groups. (c) Side and (top) view of the configuration after relaxation: all the oxygen atoms of the epoxy groups are transferred to the titanium. Titanium, carbon, and oxygen atoms are indicated in orange, dark grey, and red, respectively. We used 3-dimensional periodic boundary conditions. The simulation box is indicated via blue lines.

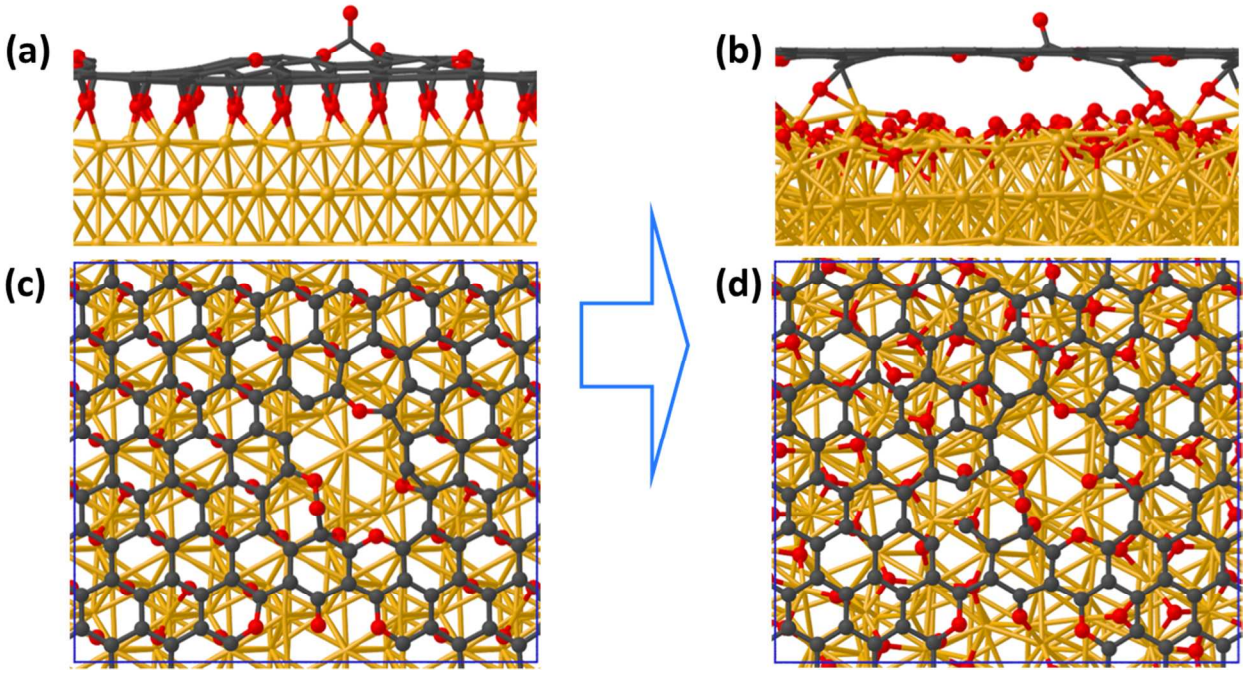

Supporting Figure S12. (a) Side and (c) top views of a larger system consisting of a single GO layer containing epoxy and carbonyl groups and a void above to a titanium surface. (b) Side and (d) top views of the configuration resulting after relaxation of (a). All the oxygen atoms initially located out of the graphene layer which were exposed to the titanium migrated at the surface of titanium layer. Only the oxygen atoms located in the voids of the GO layer are stable in the GO layer. The color code is the same as previously. The simulation box contains 144, 117, and 56 Ti, C, O atoms, respectively.

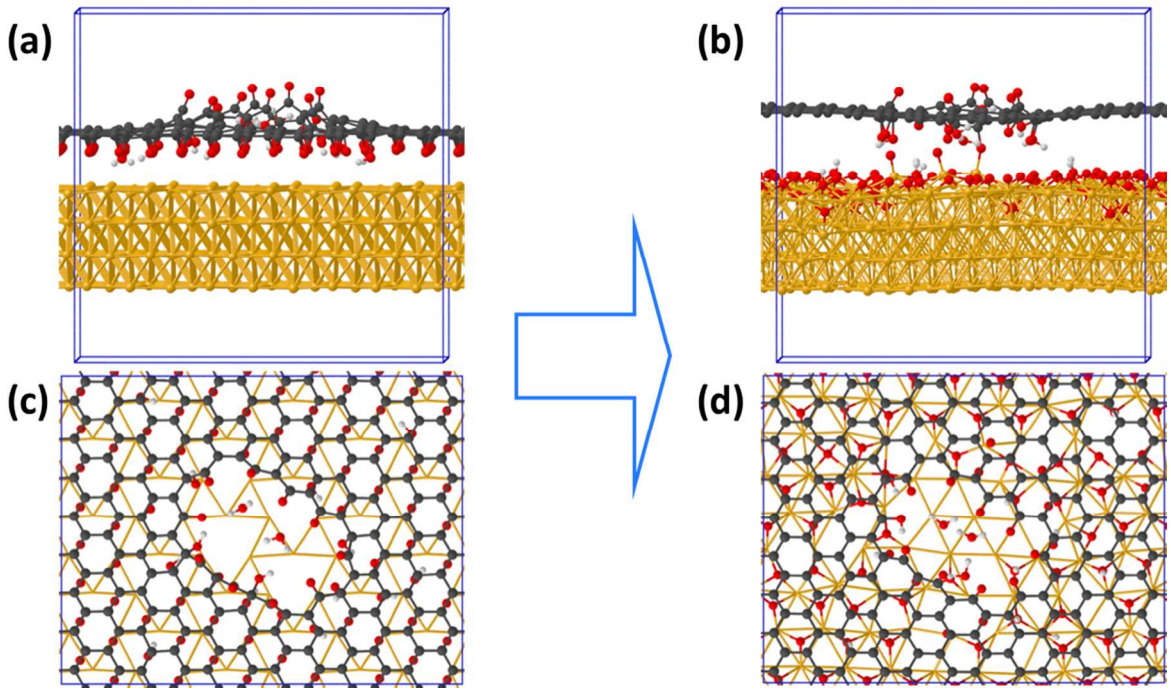

Supporting Figure S13. (a) Side and (c) top views of a larger system consisting of a single GO layer containing epoxy and carbonyl groups and a void above to a titanium surface. (b) Side and (d) top views of the configuration resulting after relaxation of (a). The majority oxygen atoms of the epoxy and hydroxyl groups bonded to the graphene side exposed to the titanium migrated at the surface of titanium layer and in a cases also below the first layer of titanium. The oxygen atoms located in the voids of the GO layer were stable in the GO layer. The simulation box contains 288, 178, 92, and 18 Ti, C, O, and H atoms, respectively. Including two water molecules added to take into account moisture. Titanium, carbon, oxygen, and hydrogen atoms are indicated in orange, dark grey, red, and light grey, respectively.

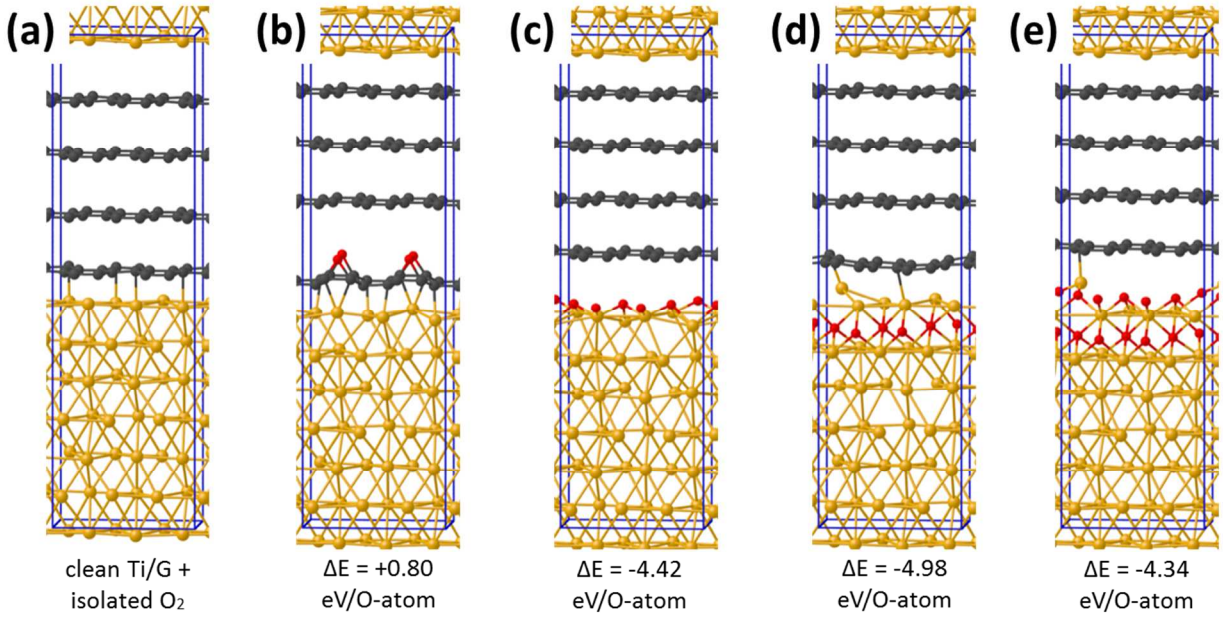

Supporting Figure S14. Energies (DFT-PBE) and structures of different geometries are given in eV/O-atom. The energy of an O_2 molecule in vacuum is taken as reference. (a) is a clean graphene/titanium interface. Structures (b) contains 4 C-O-C epoxy groups, oxygen only adsorbed on graphene. Structures (c) and (d) contain 6 O-atoms; (c) O-atoms are adsorbed at the titanium surface; (d) the O-atoms are adsorbed between the first and second layers. (e) there are 12 O-atoms, 6 adsorbed in the first titanium layer and other 6 atoms in the second titanium layer. Adsorption of oxygen atoms on clean graphene forming C-O-C epoxy groups is endothermic, see structure in Fig. S13. The energies are computed DFT-PBE level with 4x2x1 k-points sampling.

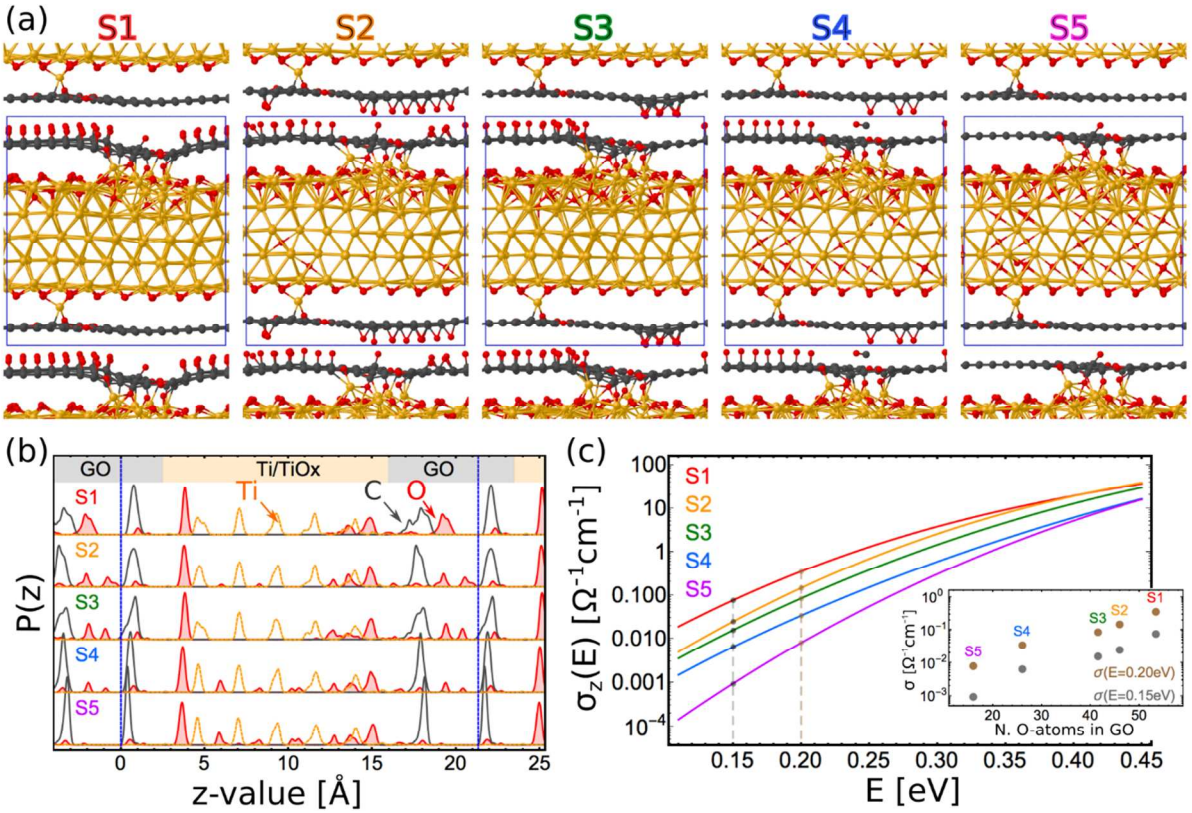

Supporting Figure S15. (a) Five models of Ti/GO interfaces made of five (two) titanium (GO) layers. Each structure contains 240, 231, and 150 Ti, C, and O atoms respectively. The normal to the Ti/GO interface is along the z-axis. Titanium, carbon, and oxygen atoms are indicated in orange, dark gray, and red, respectively. We used 3-dimensional periodic boundary conditions. The simulation box is indicated via solid blue lines. For illustrative purposes the closest atoms of the neighboring cells along z are shown. (b) Projection for each structure of atomic density on the z-axis. The projection is obtained via smearing with Gaussians (0.1 Å) the z component of the atoms of each species and is scaled by the number of atoms of each species. The color code is the same as for the atoms in (a). The amount of O atoms into the Titanium (GO) increases (decreases) from S1 to S5. Dashed blue lines indicate the box boundaries along the z-coordinate. (c) The optical conductivity σz(E) as function of the energy E for the five structures S1, S2, S3, S4, and S5 is indicated via solid red, orange, green, blue, and violet lines. The optical conductivity decreases as the oxygen is transferred from the GO to the titanium, see inset of (c), which is a plots the of values of σ at E=0.15 and 0.2 eV, see dashed gray and brown lines in (b), vs. the oxygen in GO for S1, S2, S3, S4, and S5. The number of oxygen in GO is obtained by integrating the P(z) for oxygen over the GO region (values of z from 16.0 to 23.5 Å).

Graphene oxide preparation and optical characterization

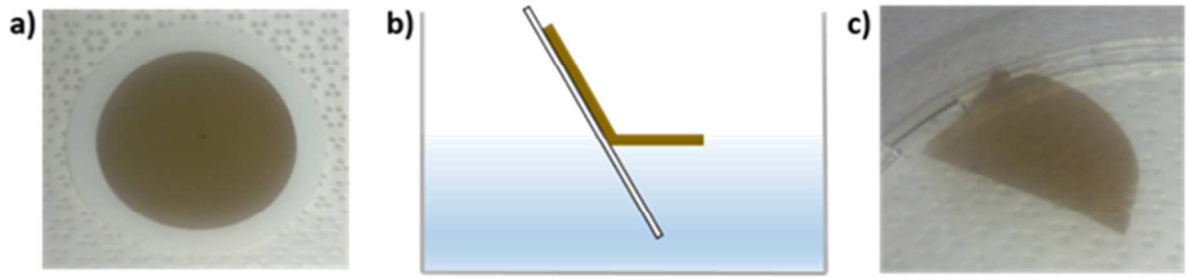

Supporting Figure S16. GO film production using the vacuum filtration method showing (a) GO film on cellulose filter after vacuum filtration, (b) illustration of delamination of GO film upon immersion in DI water and (c) GO film floating on the surface of DI-water.

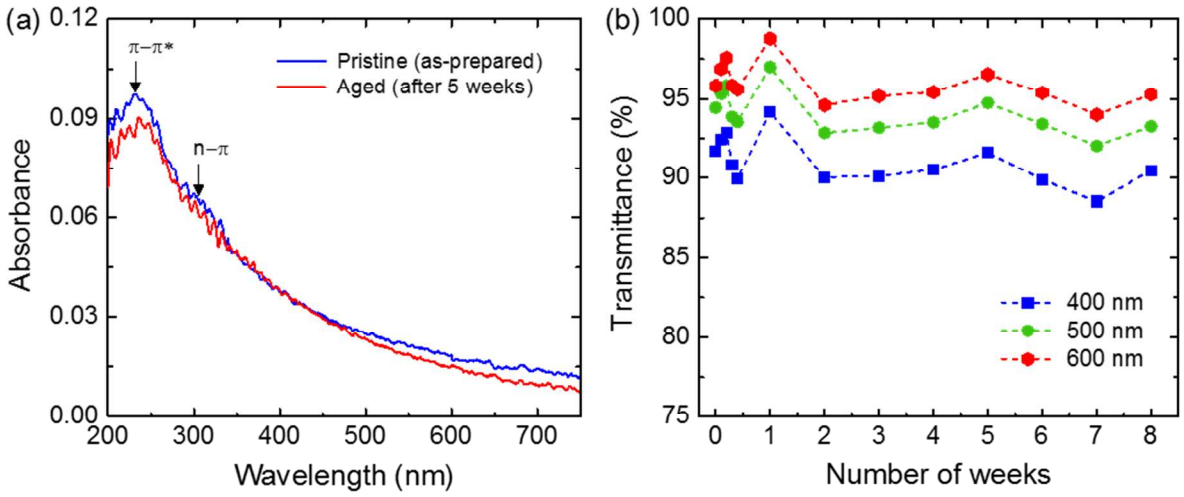

Supporting Figure S17. (a) Absorbance as a function of wavelength and (b) transmittance versus time (at three selected wavelengths) for 8 nm thick GO film (on quartz substrate). The absorbance/transmittance of the sample shows no appreciable degradation after several weeks of ambient air exposure

The effect of GO film uniformity and roughness on device performance

The electrical characteristics of GO-based memories can vary dramatically from device to device in the presence of a spatially varying GO film thickness, or other GO film inhomogeneities. There are several techniques to fabricate GO films, including spin-coating, dip-coating, drop-casting, ink-jet printing, electro-spraying and vacuum filtration. Among these deposition methods, we found that the vacuum filtration approach produces some of the smoothest GO films reported to-date with < 1.5 nm rms roughness, along with excellent film uniformity over large areas (square inches). Such a fine control of the GO film deposition process results in stable and repeatable operation of memory cells without significant performance degradation. This view is corroborated by the observation that devices fabricated from the very edge-most regions of our GO films (where the film uniformity and roughness is intrinsically poorer) had significantly worse memory characteristics, including a reduced resistance window and, importantly, very significantly reduced endurance. This is exemplified in Figure S18 where we compare the endurance characteristics of memory cells fabricated on the smooth (rms ~ 1.3 nm) and homogeneous GO film with that of cells fabricated on the relatively rough (rms ~ 4.2 nm) and inhomogeneous edge-most film regions. As can be seen (from Figure S18), for the memory cells on the uniform GO film a large resistance-window of around 1000 Ω was achieved, along with a high endurance of over 10,000 switching cycles. In contrast, devices fabricated on the relatively rough and non-uniform edge regions showed a significantly lower resistance window of around 100 Ω, and, more importantly, failed after just over 200 switching cycles (such behavior was typical of all cells fabricated on the relatively rough and non-uniform edge-most regions of our GO films). Hence, the uniformity and roughness of GO layers is of critical importance for obtaining superior device performance; it is also key to obtaining good device yields and minimal device-to-device variations, all important pre-requisites when it comes to industrial scale production.

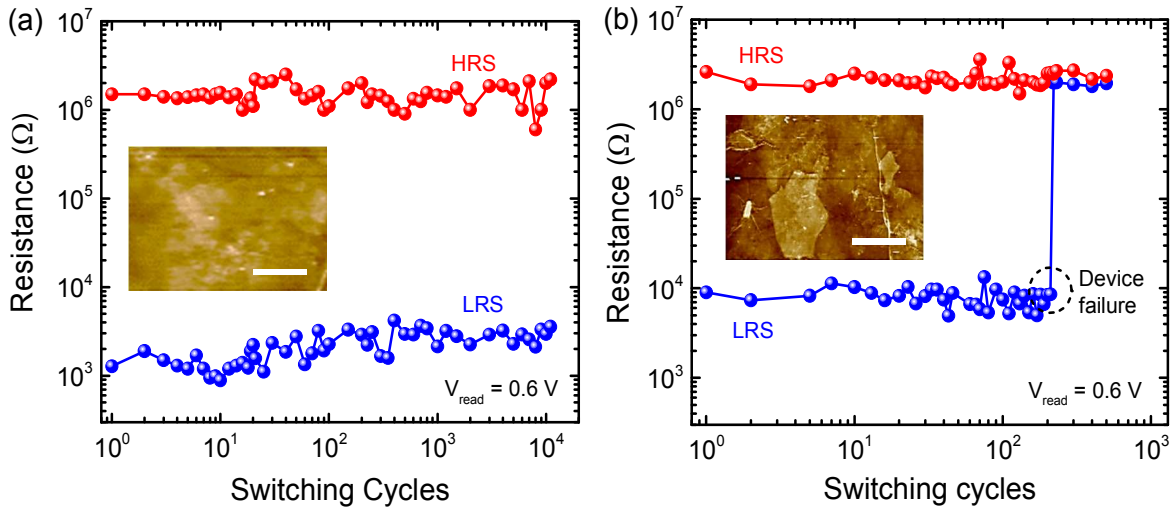

Supporting Figure S18: Endurance performance of GO memory cells with (a) smooth and uniform GO films and (b) rough and non-uniform GO films. The insets show the AFM topographic images of the respective GO films. Scale bar is 1 μm.

Supporting Information References

(1) Wright, C. D.; Hosseini, P.; Diosdado, J. A. V. Beyond Von-Neumann Computing with Nanoscale Phase-Change Memory Devices. *Adv. Func. Mater.* **2013**, *23*, 2248–2254.

(2) Kim, S. K.; Kim, J. Y.; Jang, B. C.; Cho, M. S.; Choi, S.-Y.; Lee, J. Y.; Jeong, H. Y. Conductive Graphitic Channel in Graphene Oxide-Based Memristive Devices. *Adv. Func. Mater.* **2016**.

(3) Ferrari, A. C.; Basko, D. M. Raman Spectroscopy as a Versatile Tool for Studying the Properties of Graphene. *Nat. Nanotechnol.* **2013**, *8*, 235–246.

(4) Shaikh, S. F.; Mane, R. S.; Min, B. K.; Hwang, Y. J.; Joo, O.-S. D-Sorbitol-Induced Phase Control of TiO2 Nanoparticles and Its Application for Dye-Sensitized Solar Cells. *Sci. Rep.* **2016**, *6*, 20103.

(5) Bradley, J. D. B.; Evans, C. C.; Choy, J. T.; Reshef, O.; Deotare, P. B.; Parsy, F.; Phillips, K. C.; Lončar, M.; Mazur, E. Submicrometer-Wide Amorphous and Polycrystalline Anatase TiO₂ Waveguides for Microphotonic Devices. *Opt. Express, OE* **2012**, *20*, 23821–23831.

(6) Gong, C.; Lee, G.; Bin Shan; Vogel, E. M.; Wallace, R. M.; Cho, K. First-Principles Study of Metal–Graphene Interfaces. *J. Appl. Phys.* **2010**, *108*, 123711.